JOURNAL OF ELECTROMAGNETIC ENGINEERING AND SCIENCE, VOL. 23, NO. 2, 145~153, MAR. 2023

https://doi.org/10.26866/jees.2023.2.r.154
ISSN 2671-7263 (Online) · ISSN 2671-7255 (Print)

A Novel Curved-Coil Transmitter for Quasi-omnidirectional Wireless Power Transfer

Bochao Guo[1] · Yubo Zhao[1,2] · Wei Chen[1,3,*] · Ni Guo[1] · Zijian Tian[1]

Abstract

Achieving stable power transfer by merely relying on quasi-omnidirectional couplers is challenging. In this paper, we propose a quasi-omnidirectional wireless power transfer (QWPT) system with a novel curved-coil transmitter to achieve steady transmission performance. A single power source is used to drive the transmitter's current without using a phase and current control methodology. Power is transmitted to the receiver through magnetic resonant coupling at a distance of 50 mm. Moreover, an equivalent circuit model of the curved-coil system is derived and mathematically analyzed. The mutual inductance of the proposed QWPT system is evaluated through analysis and experiments. The experimental results for the resonant coupling system confirm the theoretical analysis of the performance of the curved-coil transmitter and quasi-omnidirectional power transfer.

Key Words: Curved Coil, Magnetic Resonant Coupling, Mutual Inductance, Quasi-omnidirectional Coupler, Wireless Power Transfer (WPT).

I. Introduction

Wireless power transfer (WPT) is becoming a popular technique for diverse applications, including consumer electronic products, unmanned aerial vehicles, and implantable medical devices [1–3]. Omnidirectional charging is critical for improving system compatibility. In [4], a coupler with multiple coils nested in each other achieves stable transmission efficiency with any angular and lateral misalignment. In [5], a crossed dipole coupler with a rotating magnetic field achieves charging at any position in the same plane. In [6], a cube dipole transmitter (Tx) is used to charge multiple receivers (Rx). In [7], a cubic Tx in an optimized structure reduces costs and achieves stable transmission efficiency. In [8], a double 3D coil Tx improves the system's anti-offset ability. In [9], by adding a three-orthogonal-plane core to a Tx, the magnetic field distribution becomes uniform without increasing the Tx size or system complexity. In [10], a bowl-shaped Tx provides both spatial freedom and high efficiency, offering a promising charging solution for mobile devices. In [11], a dual-band omnidirectional 3D Tx can simultaneously offer specific advantages for the requirements of different frequencies, distances, and power. In [12], transmission performance increases with a dihedral coil angle of 80°–85°. In [13], an original double toroidal helix-coil Tx is a high-efficiency omnidirectional coupler that maintains transmission efficiency above 90% in almost the entire range of Rx positions at a transfer distance of 200 mm. Changing the structure of the Tx can make the magnetic field more uniform, while changing the structure

Manuscript received June 12, 2022 ; Revised August 10, 2022 ; Accepted December 11, 2022. (ID No. 20220612-079J)
[1]School of Mechanical Electronic and Information Engineering, China University of Mining and Technology (Beijing), Beijing, China.
[2]Shaanxi Coal Industry Co. Ltd., Shaanxi Coal Chemical Group Building, Xi'an City, China.
[3]School of Computer Science and Technology, China University of Mining and Technology, Xuzhou, China.
[*]Corresponding Author: Wei Chen (e-mail: chenwdavior@163.com)

of the Rx also enhances the coupling coefficient. In [14], a quadrature-shaped Rx realizes an angular misalignment-insensitive omnidirectional WPT system.

Algorithm makes the Tx generate a uniform rotating magnetic field [15,16]. The position of the Rx needs to be calculated [17,18] to increase transmission efficiency [19]. In [20], a uniform magnetic field is formed by rotating the Tx. In [21], a butterfly-shaped Tx significantly improves system efficiency when Rx rotates. In [22], a cubic magnetic coupler obtains a higher coupling coefficient and has high misalignment tolerance. In [23], a spatial rotating DD coil is proposed to solve the power fluctuation problem of dynamic WPT systems at medium and long transmission distances.

When the structure of the Tx changes, the magnetic field changes accordingly. Therefore, this work explores a curved circular coil and analyzes the changes in the transmission performance of coils with curved angles ranging from 90° to 180°. The 160° and 90° coils show the best transmission performance. Thus, two kinds of quasi-omnidirectional transmitters are fabricated. The 160° curved-coil Tx shows good transmission performance, while the 90° Tx shows stable transmission performance.

The rest of this paper is organized as follows. The equivalent circuit analysis is presented in Section II, which describes the mutual inductance variations in the curved coil region. The proposed curved coils are introduced with a design example in Section III. The experimental verification of the proposed concept is presented in Section IV. Section V presents the conclusions.

II. Theoretical Analysis

A WPT coupler is composed of Tx coils, relay coils, and Rx coils, and the number of coils can be adjusted according to different needs. By adjusting the number and shape of the coils, different electromagnetic fields can be generated. The equivalent circuit of the WPT system is shown in Fig. 1.

The Tx, relay, and Rx coils are tuned to a working frequency ω_0 using capacitors in a series. The Tx coils are connected to full-bridge converters (high-frequency sources), as illustrated in Fig. 1. The coupled mode theory model of the proposed WPT system can be expressed as in [24]:

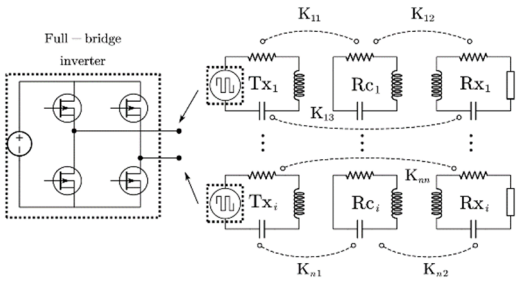

Fig. 1. Equivalent circuit of the WPT system.

$$\frac{d}{dt}\begin{bmatrix}a_1\\a_2\\\vdots\\a_n\end{bmatrix}=\begin{bmatrix}-(j\omega_1+\tau_1) & jK_{12} & jK_{13} & \cdots & jK_{1n}\\ jK_{21} & -(j\omega_2+\tau_2) & jK_{23} & \cdots & jK_{2n}\\ \vdots & \vdots & \ddots & \vdots & \vdots\\ jK_{n1} & jK_{n2} & \cdots & \cdots & -(j\omega_n+\tau_n)\end{bmatrix}\begin{bmatrix}a_1\\a_2\\\vdots\\a_n\end{bmatrix}+\begin{bmatrix}F_1\\F_2\\\vdots\\F_n\end{bmatrix}, \quad (1)$$

where $a_i = A_s e^{-j\omega t}$ denotes the energy modes of the transmitting and receiving circuits, ω_i denotes the coil's intrinsic frequency, τ_i denotes the coil's loss, $K_{ij} = K_{ji}$ $(i = j: 1, 2, \ldots, n)$ denotes the coupling coefficient between the coils, and F_i denotes the DC power supply.

By transforming Eq. (1), the power inside the Tx, relay, and Rx coils can be expressed as

$$\begin{cases} a_1 = \frac{jK_{12}a_2+jK_{13}a_3+\cdots+jK_{1n}a_n+F_1}{(j(\omega_1-\omega_0)+\tau_1)} \\ a_2 = \frac{jK_{21}a_1+jK_{23}a_3+\cdots+jK_{2n}a_n+F_2}{(j(\omega_2-\omega_0)+\tau_2)} \\ \vdots \\ a_n = \frac{jK_{n1}a_1+jK_{n2}a_2+\cdots+jK_{n(n-1)}a_{n-1}+F_n}{(j(\omega_n-\omega_0)+\tau_n)} \end{cases}. \quad (2)$$

Each coil's power is proportional to K_{ij} and inversely proportional to the coil's loss and intrinsic frequency, so the resonant system reduces the loss. When the coils' position change, K_{ij} also changes, causing fluctuations in transmission performance. When the Tx coils are perpendicular, they contain only supply power and coupled power. Therefore, they should be kept nearly perpendicular to reduce coupling effects. Relay coils, which have only coupled power, can increase the transmission range. By optimizing their structure, transmission performance can increase. The Rx coils have only coupled power. Transmission performance stability is achieved when the power load is constant. When an Rx coil changes positions, K_{ij} should remain the same to maintain a constant power load. Thus, to achieve transfer performance stability, K_{ij} should remain constant. The coupling coefficient is expressed as

$$K = \frac{\omega M}{2\sqrt{L_1 L_2}}, \quad (3)$$

where L_i denotes the coil's inductance, and M denotes the coupler's mutual inductance. Eq. (3) indicates that transmission performance is stable when M is constant. M is related to the coupler's physical structure and spatial position. The coils are coupled. To reduce the calculations and analysis, we introduce magnetic induction as

$$M = \frac{N_R \int BdS}{I}, \quad (4)$$

where I denotes the coil's current, and N_R denotes the turns of the Rx. Eq. (4) indicates that M remains stable when the magnetic induction (B) density distribution of the Tx is uniform. B is calculated as

$$B = \frac{\mu_0 \mathrm{I} N_R}{4\pi} \oint \frac{dl \times \hat{r}}{r^2}, \quad (5)$$

where I denotes the coil's current, dl denotes the line element

along the wire, $\hat{r} = \frac{(x_0-x)\hat{e}_x+(y_0-y)\hat{e}_y+(z_0-z)\hat{e}_z}{\sqrt{(x_0-x)^2+(y_0-y)^2+(z_0-z)^2}}$ denotes wire point to space point of the vector, and r denotes the distance between the source points and space points, which is (x_0, y_0, z_0). We substitute Eq. (5) with Eq. (4) as

$$M = \frac{\mu_0 N_T N_R \tilde{S}}{4\pi} \oint \frac{dl \times \hat{r}}{r^2}, \tag{6}$$

where $\tilde{S}$ denotes the area of the Rx. When the Rx moves, the total B shows little change in the Rx area, so the transmission performance is stable. Eq. (6) can be divided into three components:

$$\begin{aligned} M_x &= \frac{\mu_0 N_T N_R \tilde{S}}{4\pi}\left(\int_{y_1}^{y_2} \frac{z_0-z}{r^3} dy - \int_{z_1}^{z_2} \frac{y_0-y}{r^3} dz\right), \\ M_y &= \frac{\mu_0 N_T N_R \tilde{S}}{4\pi}\left(\int_{z_1}^{z_2} \frac{x_0-x}{r^3} dz - \int_{x_1}^{x_2} \frac{z_0-z}{r^3} dx\right), \\ M_z &= \frac{\mu_0 N_T N_R \tilde{S}}{4\pi}\left(\int_{x_1}^{x_2} \frac{y_0-y}{r^3} dx - \int_{y_1}^{y_2} \frac{x_0-x}{r^3} dy\right), \end{aligned} \tag{7}$$

where x_i, y_i, and z_i denote the range of the wire's position change. The three components of Eq. (7) allow us to clearly observe changes in the magnetic field within a certain area. The quasi-omnidirectional Tx consists of multiple curved coils. The coordinates of the points on the Tx coil-x, coil-y, and coil-z can be expressed as

$$\begin{aligned} \text{Coil-x}: &\begin{cases} x = 0 \\ y = R\cos\delta, \\ z = R\sin\delta \end{cases} \delta \in [0,\pi], \\ \text{Coil-y}: &\begin{cases} x = R\sin\varsigma \\ y = 0 \\ z = R\cos\varsigma \end{cases}, \varsigma \in [0,\pi], \\ \text{Coil-z}: &\begin{cases} x = R\cos\psi \\ y = R\sin\psi, \\ z = 0 \end{cases} \psi \in [0,\pi], \end{aligned} \tag{8}$$

where R denotes the radius of each Tx coil, and α, β, and γ denote the angular misalignment in the QWPT system rotating around the x-axis, y-axis, and z-axis, respectively. The matrix rotation along the x-axis, y-axis, and z-axis can be expressed as

$$\begin{aligned} R_x &= \begin{bmatrix} 1 & 0 & 0 \\ 0 & \cos\alpha & -\sin\alpha \\ 0 & \sin\alpha & \cos\alpha \end{bmatrix}, \\ R_y &= \begin{bmatrix} \cos\beta & 0 & \sin\beta \\ 0 & 1 & 0 \\ -\sin\beta & 0 & \cos\beta \end{bmatrix}, \\ R_z &= \begin{bmatrix} \cos\gamma & -\sin\gamma & 0 \\ \sin\gamma & \cos\gamma & 0 \\ 0 & 0 & 1 \end{bmatrix}. \end{aligned} \tag{9}$$

Taking the rotation of coil-x around the z-axis as an example,

$$\text{Coil-}\tilde{x}: \begin{cases} x = -R\cos\delta\sin\gamma \\ y = R\cos\delta\cos\gamma \\ z = R\sin\delta \end{cases}, \delta \in [0,\pi], \tag{10}$$

we substitute Eq. (10) with Eq. (8):

$$\begin{aligned} \tilde{M}_z &= \frac{\mu_0 N_T N_R \tilde{S}}{4\pi}\left(\int_0^{\pi} \frac{((y_0\text{-R}\cos\delta\cos\gamma)R\sin\delta\sin\gamma - (x_0+\text{Rcos}\delta\sin\gamma)R\sin\delta\cos\gamma)}{[(x_0+R\cos\delta\sin\gamma)^2 + (y_0\text{-R}\cos\delta\cos\gamma)^2 + (z_0\text{-R}\sin\delta)^2]^{\frac{3}{2}}} d\delta\right) \\ \tilde{M}_y &= \frac{\mu_0 N_T N_R \tilde{S}}{4\pi}\left(\int_0^{\pi} \frac{((x_0+R\cos\delta\sin\gamma)R\cos\delta - (z_0 - R\sin\delta)R\sin\delta\sin\gamma)}{[(x_0+R\cos\delta\sin\gamma)^2 + (y_0\text{-R}\cos\delta\cos\gamma)^2 + (z_0\text{-R}\sin\delta)^2]^{\frac{3}{2}}} d\delta\right), \\ \tilde{M}_z &= \frac{\mu_0 N_T N_R \tilde{S}}{4\pi}\left(\int_0^{\pi} \frac{((y_0\text{-R}\cos\delta\cos\gamma)R\sin\delta\sin\gamma - (x_0+\text{Rcos}\delta\sin\gamma)R\sin\delta\cos\gamma)}{[(x_0+R\cos\delta\sin\gamma)^2 + (y_0\text{-R}\cos\delta\cos\gamma)^2 + (z_0\text{-R}\sin\delta)^2]^{\frac{3}{2}}} d\delta\right). \end{aligned} \tag{11}$$

We have established the mathematical model of the QWPT system, which can guarantee transmission performance stability as long as the average B is constant. To find the optimal combination, we simulate and analyze the combinations of different numbers of curved coils.

III. The Proposed WPT Tx

Although increasing the number of Tx coils can make B more uniform, many coils degrade transmission performance. We need to analyze the magnetic field distribution of coils with different curved angles and determine the arrangement and number of coils according to the characteristics of the magnetic field. The coil's curved angles range from 90° to 180°. An angle cannot be less than 90° because the current's direction is opposite within 90°, which will reduce the absolute value of B. As shown in Fig. 2, the coil angle changes from 180° to 90° by 10° each time.

The curved coil divides space into two parts: a wide-angle area (WAA) and a narrow-angle area (NAA). When the central point of the Rx is around θ = 90° and φ = 0°–360° (θ movement), the B value of the NAA increases, so the mutual inductance increases. The opposite occurs in the WAA. When the central point of the Rx is around θ = 0°–360° and φ = 90° (φ movement), the curved coils are equally spaced. As the curved angle narrows, the mutual inductance increases in the front of the curved coil (FCC) and decreases in the reverse of the curved

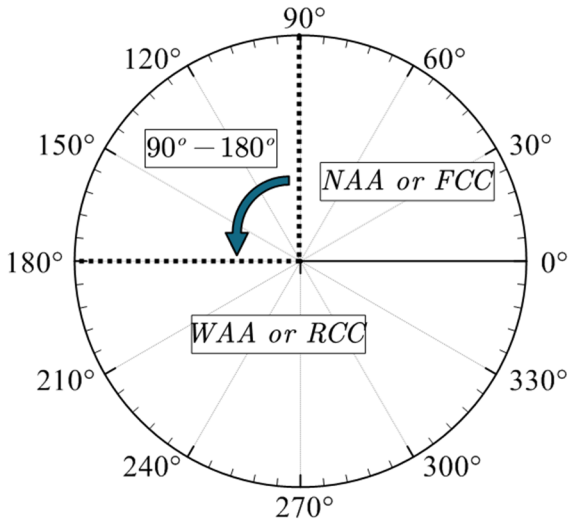

Fig. 2. Different areas of a curved coil.

coil (RCC). Therefore, we need to analyze the B value in both directions.

As shown in Fig. 3(a), the variation of B indicates that the transmission performance of the 90° curved coil is better than that of the other coils. The variation of the WAA's B is smaller than that of the NAA. Therefore, the WAA can be used only to enhance transmission performance. However, the 90° curved coil also covers the smallest area, so good transmission performance is achieved in a limited area.

As shown in Fig. 3(b), the φ movement divides the space into two equal parts, and the B value of the FCC is greater than that of the RCC. This change is consistent with the 180° coil in the Tx design, but the transmission performance of the FCC is enhanced.

We can conclude the following:

- The curved coil can enhance the transmission performance of the front area.
- As the curved angle widens, the area of high transmission performance shrinks.
- The φ movement divides the space evenly, but the θ movement does not.

To design the quasi-omnidirectional Tx, we verify the above conclusions by conducting experiments on the curved coils.

The power and efficiency trends shown in Fig. 4 are similar to those shown in Fig. 3(a). In the NAA, narrower curved angles have better transmission performance. The transmission performance of the 180° coil is significantly weaker than that of the other coils, and the coverage area of the 90° coil is the smallest. In the WAA, the 160° coil shows the best transmission performance and the largest coverage area. Therefore, the 160° coil is the optimal coil for the θ movement.

The power and efficiency trends shown in Fig. 5 are similar to those shown in Fig. 3(b). The space is divided into two equal parts. The transmission performance of the FCC is better than that of the RCC. In the FCC, the 90° coil has better transmission performance, whereas in the RCC, the 180° coil has better performance. Their coverage areas are basically the same. We can conclude that the 90° coil is the optimal coil for the φ movement.

In summary, the 160° coil is the optimal coil for the θ movement, and the 90° coil is the optimal coil for the φ movement. Therefore, we design two curved-coil Txs, CTx1 and CTx2, as

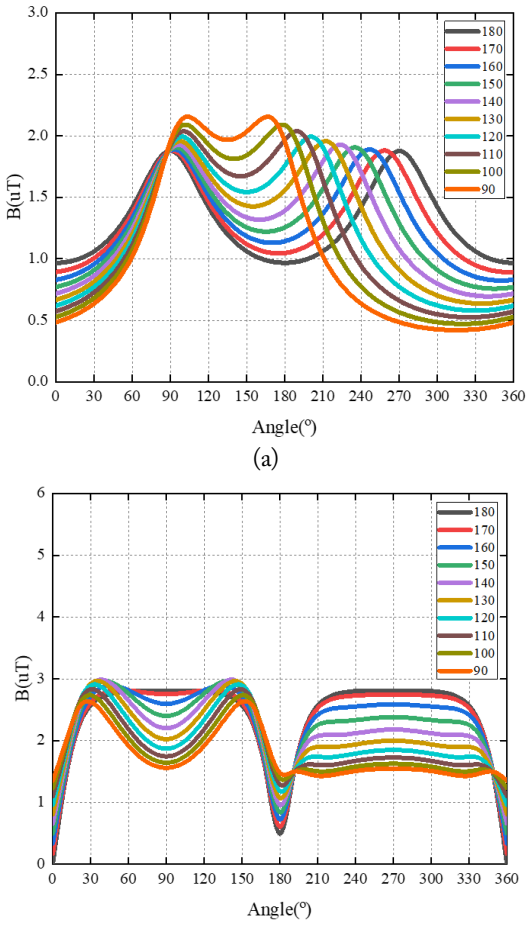

Fig. 3. Variation of B for two orbiting motions: (a) θ movement and (b) φ movement.

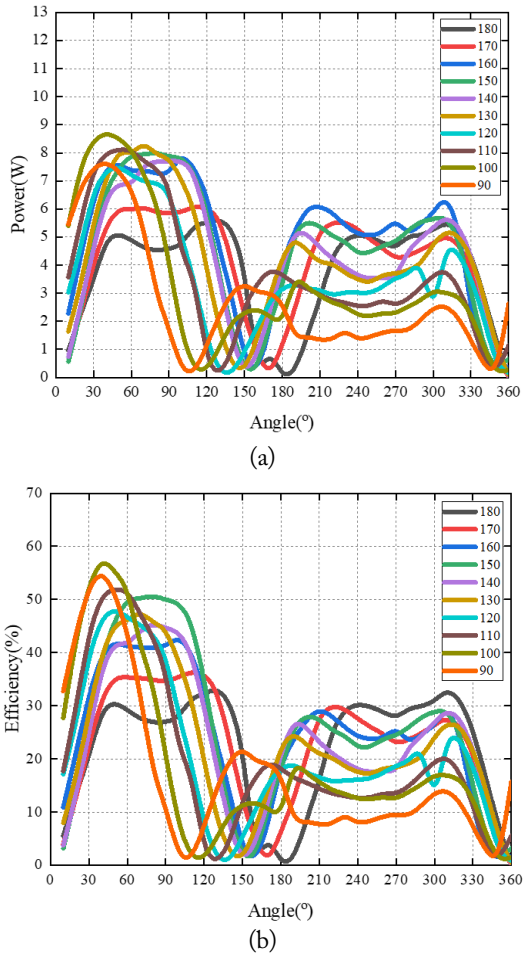

Fig. 4. Transmission performance of the θ movement: (a) transmission power and (b) efficiency.

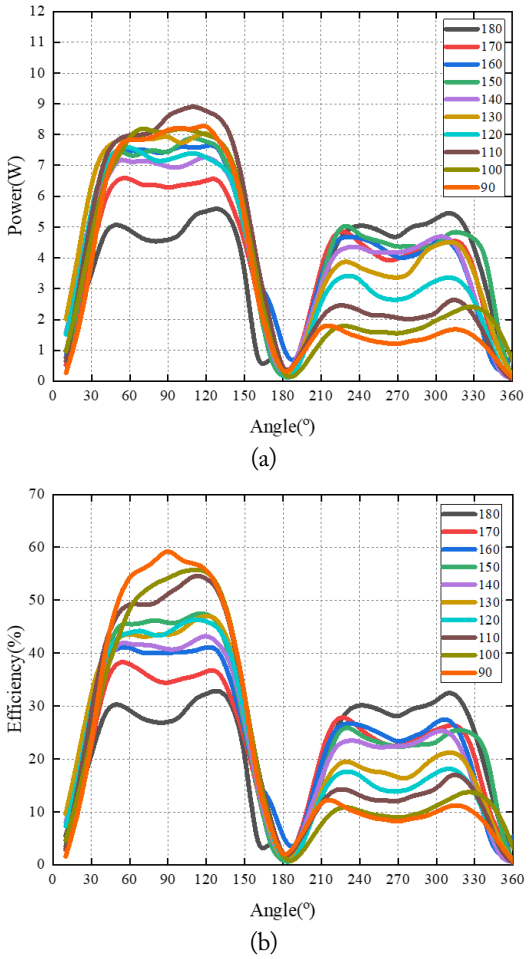

Fig. 5. Transmission performance of the φ movement: (a) transmission power and (b) efficiency.

shown in Fig. 6. CTx1 is composed of four 90° coils. Two opposite coils form a pair, and the current of the opposite coils is reversed, canceling out the magnetic field. The magnetic field of the 90° coil is small in the RCC, so its influence is reduced. Two pair are perpendicular to each other, as shown in Fig. 6(a). CTx2 is composed of four 160° coils. To expand the effective charging area and reduce the angle of the same current, the coils are combined irregularly. In each pair, one side of one coil overlaps with one side of the other. Moreover, one side of one pair overlap with one side of the other, as shown in Fig. 6(b).

IV. Experimental Verification

Based on the principles of the curved-coil Tx presented above, we evaluate quasi-omnidirectional Tx prototypes. The radius of the coils is set to 50 mm, while the radius of the copper wire is 2 mm. The current on each side of the curved coil is supplied by a single source and generates a magnetic field surrounding the resonant loop. Fig. 7 shows the top view of the magnetic field of the curved-coil Tx. The B distribution of CTx1 is sparse but relatively uniform, whereas that of CTx2 is denser but has two

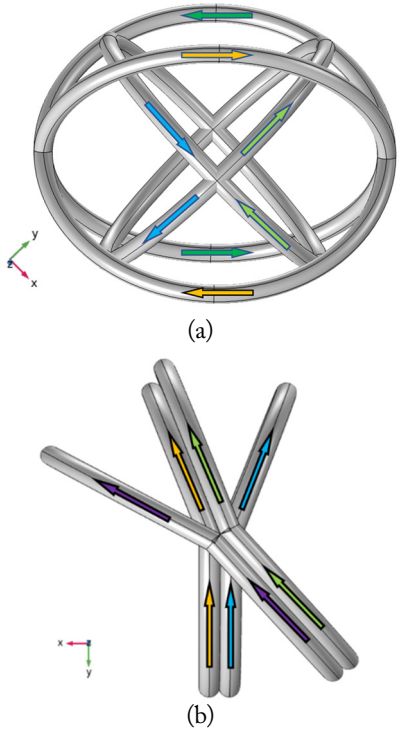

Fig. 6. Quasi-omnidirectional couplers in a 3D view: (a) CTx1 and (b) CTx2. Arrows of the same color represent the current direction of the same coil.

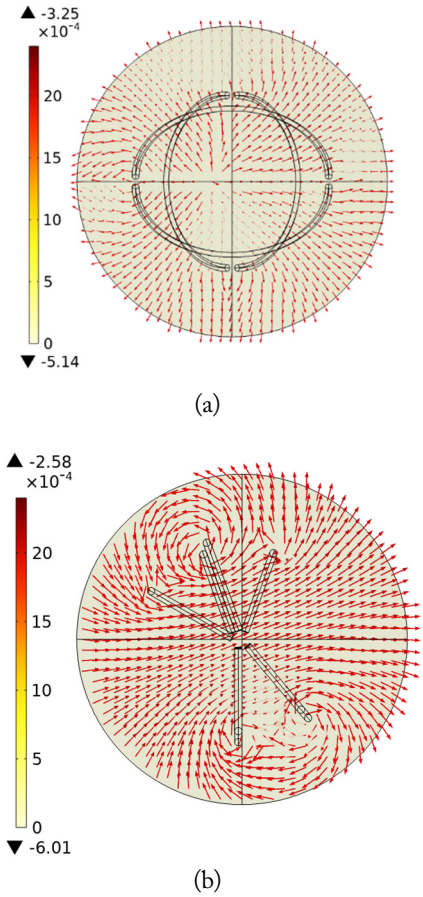

Fig. 7. Magnetic field distributions of (a) CTx1 and (b) CTx2.

sparse areas. CTx2 has better transmission performance than CTx1, but it also has a dead zone. The reason for this is that the direction of the rotating magnetic field is parallel to the Rx at the dihedral angle of the same current. The transmission performance of CTx1 is relatively stable. The simulated distributions of the magnetic field vectors generated by the Tx coils agree well with the theoretical analysis presented above.

Fig. 8 shows the experimental equipment used to verify the proposed QWPT system. The CTxs are shown in Fig. 8(a)–8(c). The coils' parameters are shown in Table 1. The CTxs are made from a Litz wire. As shown in Fig. 8(d), the CTxs are placed in the *xoy* plane. All coils are tuned to the design frequency using NPO capacitors. The experimental frequency is set to 100 kHz, which is slightly different from the design frequency due to the use of a compensation capacitor. For the power source, a full-bridge inverter is built using four MOSFETs (IRLL024NPbF). The load resistance is connected to the Rx coil. The input voltage (V_{in}) is 5 V, and the load is 1 Ω. The input current (I_{in}), VRMS, and IRMS of the load are recorded at 10° intervals to calculate the transmission power and efficiency, as shown in Fig. 9. The Rx is manually rotated counterclockwise around the origin of coordinate in the *xoy* plane from $\theta = 0°$ to $\theta = 360°$ on coordinate paper, with the distance between the Rx and the center fixed at 50 mm.

Table 1. Coil parameters

Parameter	Value
Rx coil inductance	8.1 μH
Rx coil compensation capacitor	311 μF
CTx1 inductance	27.3 μH
CTx1 compensation capacitor	92.8 μF
CTx2 inductance	64.3 μH
CTx2 compensation capacitor	40 μF
CTx1s inductance	33.9 μH
CTx1s compensation capacitor	74.8 μF

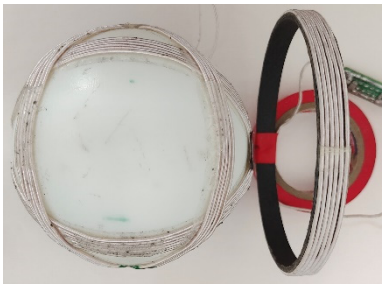

(a)

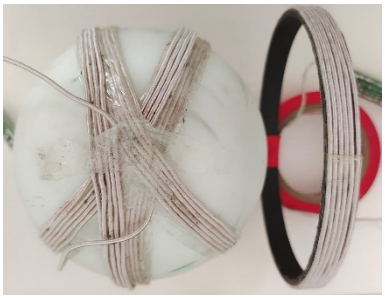

(b)

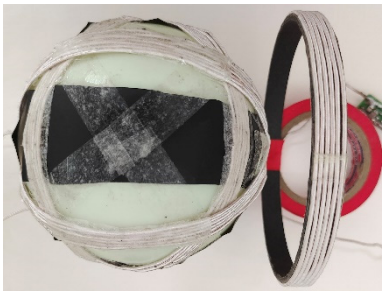

(c)

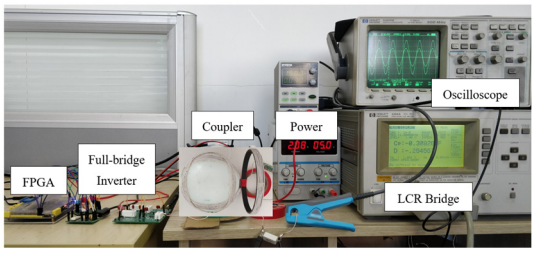

(d)

Fig. 8. Experimental equipment: (a) CTx1, (b) CTx2, (c) CTx1s, and (d) experimental platform.

The experimental transmission performance results are shown in Fig. 10. Efficiency is measured from the DC power sources to the AC load.

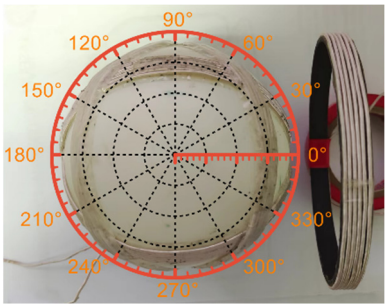

Fig. 9. Sketch map of the experimental measurement.

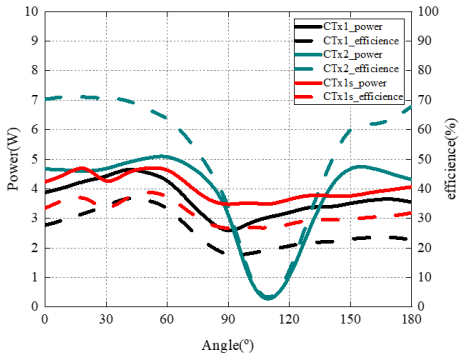

Fig. 10. Transmission performance of the three CTxs.

The transmission performance of CTx1 is basically stable at 0°–360°, but its average efficiency is 27%. The reason for its inefficiency is that the magnetic inductions of opposite coils cancel each other out. CTx1 does not have the same current direction, so dead zones are avoided. To reduce the influence of the opposite coils, we add a magnetic shielding material to CTx1, obtaining CTx1s, which has significantly improved transmission performance. Because the bent magnetic shielding material will shark, we cannot cover all the spheres, but we demonstrate that adding a magnetic shielding material can improve transmission performance.

CTx2 has stable transmission performance at 30°–60° and 150°–330°, but it also has two dead zones at 0° and 120° because the magnetic field is parallel to the Rx at the dihedral angle of the same current, and the magnetic inductions of the other coils do not fill the two points. Adjusting the combination of the 160° coils will increase the number or size of dead zones. Due to the existence of dead zones, the magnetic field of CTx2 is not uniform. The dead zones are located between two Tx coils with the same current direction. The adjacent coils with the same current direction cause the B of Tx to be parallel to the Rx, so the system cannot transmit power.

A comparison between the proposed QWPT systems and previously proposed structures is presented in Table 2. Previously proposed structures are based on orthogonal coils that require complex control methods and multiple sources [25–27]. On the other hand, the CTxs presented in this article offer a completely 2D omnidirectional WPT system with a single source.

V. Conclusion

This paper presents a new quasi-omnidirectional Tx based on curved coils. An equivalent circuit is derived, and a mathematical analysis is performed to specify the resonant coupling operation. The 160° coil is the optimal coil for the θ movement, while the 90° coil is the optimal coil for the φ movement. CTx2 has an average efficiency of 63% with 4.45 W at 30°–60° and 150°–330°, but it also has two dead zones. CTx1 can deliver power of 4.41 W to the Rx coil arranged around it with an efficiency of approximately 27% at an operating frequency of 100 kHz and an optimal separation of 50 mm. By adding a magnetic shielding material, the efficiency can rise to 32%. Low-cost fabrication without using a current control methodology was implemented to verify the practical design of the quasi-omnidirectional curved-coil Tx with a single Rx.

CTx1 does not have a dead zone but has relatively low efficiency, the efficiency of the QWPT system can be increased by placing metamaterial slabs around the CTx1 coil. The FCC of the curved coil can enhance transmission performance, so it can be used in other charging fields.

This work was supported by the National Natural Science Foundation of China (No. 52074305 and 51874300).

Table 2. Comparison of QWPT systems

Study	Coil shape	Sources	Control method	Frequency	Tx/Rx dimensions (cm)	Tx-Rx distance (cm)	Efficiency (%)	Output power (W)
Chen et al. [25]	Cylinder	Multiple	Phase-shifted angle control	100 kHz	22 × 30 / 22 × 30	25	60 (Avg.)	Max: 40 Min: 25
Tan et al. [26]	Cylinder	Multiple	None	85 kHz	-	-	-	Max: 5.6 Min: 4
Ha-Van et al. [27]	Cylinder	Single	None	6.78 MHz	15 / 10	10	72	13.5
This work								
CTx1	Sphere	Single	None	100 kHz	5/5	5	Max: 37 Min: 17	Max: 4.7 Min: 2.4
CTx2	Sphere	Single	None	100 kHz	5/5	5	Max: 71 Min: 1	Max: 5.2 Min: 0
CTx1s	Sphere	Single	None	100 kHz	5/5	5	Max: 39 Min: 26	Max: 4.9 Min: 3.4

References

[1] S. H. Kang and C. W. Jung, "Magnetic resonant wireless power transfer with rearranged configurations," *Journal of Electromagnetic Engineering and Science*, vol. 17, no. 2, pp. 76-85, 2017.

[2] J. Park, J. Kim, Y. Shin, B. Park, W. S. Kim, S. J. Cheong, and S. Ahn, "Toroidal-shaped coils for a wireless power

transfer system for an unmanned aerial vehicle," *Journal of Electromagnetic Engineering and Science*, vol. 19, no. 1, pp. 48-55, 2019.

[3] X. Dai, X. Li, Y. Li, and A. P. Hu, "Maximum efficiency tracking for wireless power transfer systems with dynamic coupling coefficient estimation," *IEEE Transactions on Power Electronics*, vol. 33, no. 6, pp. 5005-5015, 2018.

[4] O. Jonah, S. V. Georgakopoulos, and M. M. Tentzeris, "Orientation insensitive power transfer by magnetic resonance for mobile devices," in *Proceedings of the 2013 IEEE Wireless Power Transfer (WPT)*, Perugia, Italy, 2013, pp. 5-8.

[5] B. H. Choi, E. S. Lee, Y. H. Sohn, G. C. Jang, and C. T. Rim, "Six degrees of freedom mobile inductive power transfer by crossed dipole Tx and Rx coils," *IEEE Transactions on Power Electronics*, vol. 31, no. 4, pp. 3252-3272, 2016.

[6] C. Rong, X. He, M. Liu, Y. Wang, X. Liu, C. Lu, Y. Zeng, and R. Liu, "Omnidirectional free-degree wireless power transfer system based on magnetic dipole coils for multiple receivers," *IEEE Access*, vol. 9, pp. 81588-81600, 2021.

[7] N. Ha-Van and C. Seo, "Analytical and experimental investigations of omnidirectional wireless power transfer using a cubic transmitter," *IEEE Transactions on Industrial Electronics*, vol. 65, no. 2, pp. 1358-1366, 2018.

[8] W. Han, K. T. Chau, C. Jiang, W. Liu, and W. H. Lam, "Design and analysis of quasi-omnidirectional dynamic wireless power transfer for fly-and-charge," *IEEE Transactions on Magnetics*, vol. 55, no. 7, article no. 8001709, 2019. https://doi.org/10.1109/TMAG.2019.2895716

[9] H. R. Cha, K. R. Park, T. J. Kim, and R. Y. Kim, "Design of magnetic structure for omnidirectional wireless power transfer," *IEEE Transactions on Power Electronics*, vol. 36, no. 8, pp. 8849-8860, 2021.

[10] J. Feng, Q. Li, F. C. Lee, and M. Fu, "Transmitter coils design for free-positioning omnidirectional wireless power transfer system," *IEEE Transactions on Industrial Informatics*, vol. 15, no. 8, pp. 4656-4664, 2019.

[11] C. Lu, X. Huang, X. Tao, X. Liu, C. Rong, Y. Zeng, and M. Liu, "Design and analysis of an omnidirectional dual-band wireless power transfer system," *IEEE Transactions on Antennas and Propagation*, vol. 69, no. 6, pp. 3493-3502, 2021.

[12] J. Li, Y. Yang, H. Yan, C. Liu, L. Dong, and G. Wang, "Quasi-omnidirectional wireless power transfer for a sensor system," *IEEE Sensors Journal*, vol. 20, no. 11, pp. 6148-6159, 2020.

[13] P. Jayathurathnage, X. Dang, C. R. Simovski, and S. A. Tretyakov, "Self-tuning omnidirectional wireless power transfer using double-toroidal helix coils," *IEEE Transactions on Industrial Electronics*, vol. 69, no. 7, pp. 6828-6837, 2022.

[14] Z. Zhang and B. Zhang, "Angular-misalignment insensitive omnidirectional wireless power transfer," *IEEE Transactions on Industrial Electronics*, vol. 67, no. 4, pp. 2755-2764, 2020.

[15] B. J. Che, G. H. Yang, F. Y. Meng, K. Zhang, J. H. Fu, Q. Wu, and L. Sun, "Omnidirectional non-radiative wireless power transfer with rotating magnetic field and efficiency improvement by metamaterial," *Applied Physics A*, vol. 116, pp. 1579-1586, 2014.

[16] Q. Zhu, M. Su, Y. Sun, W. Tang, and A. P. Hu, "Field orientation based on current amplitude and phase angle control for wireless power transfer," *IEEE Transactions on Industrial Electronics*, vol. 65, no. 6, pp. 4758-4770, 2018.

[17] D. Lin, C. Zhang, and S. R. Hui, "Mathematical analysis of omnidirectional wireless power transfer—Part-I: Two-dimensional systems," *IEEE Transactions on Power Electronics*, vol. 32, no. 1, pp. 625-633, 2017.

[18] D. Lin, C. Zhang, and S. R. Hui, "Mathematic analysis of omnidirectional wireless power transfer—Part-II: Three-dimensional systems," *IEEE Transactions on Power Electronics*, vol. 32, no. 1, pp. 613-624, 2017.

[19] H. Wang, C. Zhang, Y. Yang, H. W. R. Liang, and S. Y. R. Hui, "A comparative study on overall efficiency of two-dimensional wireless power transfer systems using rotational and directional methods," *IEEE Transactions on Industrial Electronics*, vol. 69, no. 1, pp. 260-269, 2022.

[20] G. Liu, B. Zhang, W. Xiao, D. Qiu, Y. Chen, and J. Guan, "Omnidirectional wireless power transfer system based on rotary transmitting coil for household appliances," *Energies*, vol. 11, no. 4, article no. 878, 2018. https://doi.org/10.3390/en11040878

[21] N. Ha-Van and C. Seo, "Modeling and experimental validation of a butterfly-shaped wireless power transfer in biomedical implants," *IEEE Access*, vol. 7, pp. 107225-107233, 2019.

[22] Y. Wang, P. Gu, Y. Yao, and D. Xu, "Analysis and design of cubic magnetic coupler for high distance-to-diameter ratio IPT systems," *IEEE Transactions on Industrial Electronics*, vol. 69, no. 1, pp. 409-419, 2022.

[23] L. Tan, R. Zhong, Z. Tang, T. Meng, and X. Huang, "Power stabilisation scheme design using spatial rotating coil based on magnetic field aggregation," *IET Power Electronics*, vol. 13, no. 12, pp. 2511-2522, 2020.

[24] Z. Wei and B. Zhang, "Transmission range extension of PT-symmetry-based wireless power transfer system," *IEEE Transactions on Power Electronics*, vol. 36, no. 10, pp. 11135-11147, 2021.

[25] X. Chen, X. Fu, C. Jiang, C. Pei, and F. Liu, "Magnetic-field-model and circuit-model based analysis of three-

phase magnetically coupled resonant wireless power transfer systems with cylinder-shaped coils," *Journal of Power Electronics*, vol. 18, no. 4, pp. 1154-1164, 2018.

[26] L. Tan, R. Zhong, Z. Tang, T. Huang, X. Huang, T. Meng, et al., "Power stability optimization design of three-dimensional wireless power transmission system in multi-load application scenarios," *IEEE Access*, vol. 8, pp. 91843-91854, 2020.

[27] N. Ha-Van, Y. Liu, P. Jayathurathnage, C. R. Simovski, and S. A. Tretyakov, "Cylindrical transmitting coil for two-dimensional omnidirectional wireless power transfer," *IEEE Transactions on Industrial Electronics*, vol. 69, no. 10, pp. 10045-10054, 2022.

Bochao Guo

received a B.S. degree from Qing Gong College, North China University of Science, Tangshan, China, in 2016 and an M.S. degree from the Jiangxi University of Science and Technology, Ganzhou, China, in 2019. He is currently pursuing a Ph.D. in information engineering at the China University of Mining and Technology, Beijing. His current research interests include wireless power transfer and electromagnetic compatibility.

Yubo Zhao

received a B.S. degree in communication engineering and an M.S. degree in business administration from the Xi'an University of Science and Technology, Shaanxi, China, in 1994 and 2013, respectively. He is currently a Ph.D. candidate in the Department of Information and Communication Engineering of the China University of Mining and Technology, Beijing. He has engaged in research and practice in the area of coal mine safety monitoring and communication. He is a senior communication engineer currently committed to promoting the holistic intelligent development of Shaanxi Coal Industry Co. Ltd.

Wei Chen

received a B.S. degree in medical imaging and an M.S. degree in paleontology and stratigraphy from the China University of Mining and Technology, Xuzhou, China, in 2001 and 2005, respectively. He obtained a Ph.D. degree in communications and information systems from the China University of Mining and Technology, Beijing, China, in 2008. In 2008, he joined the School of Computer Science and Technology, China University of Mining and Technology, where he is currently a professor. He is a member of IEEE and EAI. He has published more than 80 research papers. He is an associate editor of the journal, *Array*. His research interests include machine learning, image processing, and computer networks.

Ni Guo

received a B.S. degree from Datong University, Shanxi, China, in 2016. She is currently pursuing a Ph.D. degree at the School of Mechanical Electronic and Information Engineering, China University of Mining and Technology, Beijing, China. Her research interests include data mining, the Internet of Things, and artificial intelligence.

Zijian Tian

received a B.S. degree from the Xi'an University of Science and Technology, Shaanxi, China, and an M.S. degree from the China University of Mining and Technology, Beijing, China, in 1986 and 1995, respectively. He obtained a Ph.D. degree in communications and information systems from the China University of Mining and Technology, Beijing, China, in 2003. In 2003, he joined the School of Mechanical Electronic and Information Engineering, China University of Mining and Technology (Beijing), where he is currently a professor. He is a member of the National Expert Group of Safety Production and a member and convener of the Expert Committee of Information and Automation, a branch of the Coal Industry Committee of Technology. His current research interest is wireless power transmission.